Enhanced Photocurrent Quantum Yield by Electronic Interaction between Zinc Porphyrin and Rhodamine B Molecules in Al/Dye/Au Sandwich-Type Solar Cell

Kohshin Takahashi,* Jyun-ichi Nakamura, Takahiro Yamaguchi, Teruhisa Komura, Shoji Ito,† and Kazuhiko Murata†

Department of Chemistry and Chemical Engineering, Faculty of Engineering, Kanazawa University, Kodatsuno, Kanazawa 920, Japan

Received: September 19, 1996; In Final Form: November 17, 1996[⊗]

The enhanced photocurrent is observed with the mixed solid of 5,10,15,20-tetraphenylporphyrinatozinc (Zntpp) and rhodamine B (RhB) compared with the pure Zntpp and RhB solids in Al/dye/Au sandwich-type solar cell. The photocurrent quantum yield has a maximum at the mixing ratio (R) of 0.5−0.8 defined as the molar ratio of porphyrin to total dye. The enhancement arises from the decrease of the series resistance by 2 orders of magnitude upon mixing Zntpp and RhB for the best cells. For the Al/mixed solid ($R = 0.57$)/Au cell, the short-circuit photocurrent quantum yield (ϕ) of 14.7%, the open-circuit photovoltage (V_{oc}) of 0.90 V, the fill factor (ff) of 0.18, and the energy conversion yield (η) of 0.82% are obtained when illuminated with 440 nm monochromatic light of 14.7 μW cm^{-2} intensity at the Al/dye interface, and the values of $\phi = 9.1\%$, $V_{oc} = 0.90$ V, ff = 0.19, and $\eta = 0.72\%$ are obtained when the sample is illuminated with 570 nm monochromatic light of 32.4 μW cm^{-2} intensity. It is found from the absorption spectra of the mixed film and the cyclic voltammograms of the mixture in dichloromethane that a ground-state complex is formed between Zntpp and RhB molecules. Larger specific conductivity is obtained with the mixed solids of $R =$ 0.6−0.8 than with the pure Zntpp and RhB solids because the ground-state complex is easily oxidized and holes as the majority carrier consequently increase. In addition, the enhancement of the photocurrent of the solar cell made up of the mixed solid is interpreted in terms of the increased potential gradient in the Schottky barrier and the ease of the charge separation of an excited state formed from the ground-state complex.

Introduction

Much effort has been expended to convert solar energy effectively to electric energy by organic solar cells. The organic solar cells have especially attracted attention since Tang reported a relatively large power conversion efficiency for a two-layer organic photovoltaic cell fabricated from copper phthalocyanine and a perylene tetracarboxylic derivative.[1]

The photovoltaic properties of chlorophyll *a* have been widely studied in relation to the primary process of photosynthesis in plants,[2−8] but the energy conversion yield was low. The chlorophyll *a* molecules were mixed with various photosynthetic pigments to reproduce partially the conditions encountered in vivo.[9,10] However the yield was not improved. A well-designed molecular system such as a photoreaction center in plants has been produced by the Langmuir−Blodgett technique.[11,12] In their model systems, an electron donor, an acceptor, and an antenna pigment were arranged on a molecular scale, since they fully function for the energy transfer and the photoinduced electron transfer.

Phthalocyanines,[13−16] porphyrins,[17,18] and merocyanines[19−21] have been investigated as available organic materials for the photoelectric conversion. Popovic et al.[22] inferred by measuring an electric field-induced fluorescence quenching of phthalocyanines that a photoinduced charge-transfer state was formed by an external field and that it dissociated to free carriers. Saito et al.[23] also studied the photocarrier generation processes of phthalocyanines by measuring the temperature dependence of the transient photocurrent, lifetime of the precursor of the free carrier, and electroabsorption spectra. They indicated that the nature of the excited states, namely, the strength of the charge-transfer interaction, should dominate the free carrier generation efficiency.

To enhance the efficiency of photoinduced charge separation, dyes mixed with a donor or an acceptor have been examined. Kearns et al.[24] found that the addition of *o*-chloranil to the surface of phthalocyanine films was allowed to increase remarkably dark- and photoconductivities. Furthermore, a remarkable improvement of photovoltaic properties was observed with phthalocyanine doped with 2,4,7-trinitrofluorenone or *o*-chloranil,[25] merocyanine adsorbed with chlorine gas,[26] and porphyrins mixed with *o*-chloranil or iodine.[27,28] An increase of hole concentration by the electron transfer from the dyes to the acceptors in the dark and under illumination and an ease of the charge separation in the excited state of the mixed solids should be responsible for the improvement. Hiramoto et al.[29] investigated an extrinsic carrier photogeneration in a perylene pigment mixed with a small amount of phthalocyanine by the electric field-induced fluorescence quenching. They assumed that the effective carrier photogeneration was ascribed to the photogeneration of geminate ion pairs through perylene/phthalocyanine molecular contacts.

We have been investigating the photovoltaic properties of various porphyrin solar cells.[28,30−32] We previously reported that an enhancement of photocurrent was observed with a porphyrin heterodimer consisting of 5,10,15-tri(4-chlorophenyl)-20-(3-pyridyl)porphyrin ($H_2pyp_3p(Cl)$) and 5,10,15,20-tetra(2,5-dimethoxyphenyl)porphyrinatozinc ($Zntpp(OMe)_2$),[30] which imitated the so-called special pair in the photosynthetic reaction center of *Rhodopseudomonas viridis*.[33] This suggested that H_2-$pyp_3p(Cl)$ and $Zntpp(OMe)_2$ in the heterodimer acted as an acceptor and a donor under illumination, respectively, and that a photoinduced charge-transfer state was easily formed. In this

† Tsukuba Research Laboratory, Nippon Shokubai Co., Ltd., Kannondai, Tsukuba 305, Japan.

[⊗] Abstract published in *Advance ACS Abstracts,* January 15, 1997.

S1089-5647(96)02887-8 CCC: $14.00

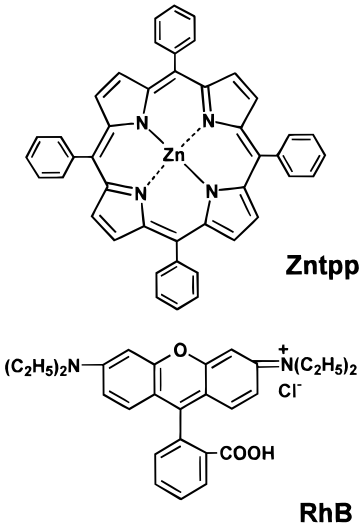

Figure 1. Structures and abbreviations of dyes.

paper, the photovoltaic properties of the mixed solid of 5,10,-15,20-tetraphenylporphyrinatozinc (Zntpp) as the donor and rhodamine B (RhB) as the acceptor have been investigated by the Al/dye/Au sandwich-type cell. The molecular structures of Zntpp and RhB are shown in Figure 1. We report that a large electronic interaction between Zntpp and RhB molecules induces the enhancement of the photocurrent and that visible light is widely used for the energy conversion because Zntpp and RhB have different absorption bands.

Experimental Section

5,10,15,20-Tetraphenylporphyrinatozinc was synthesized by literature methods[34,35] and purified by column chromatography on alumina and silica gel. Rhodamine B purchased from Kanto Chemical was recrystallized twice in acetic acid.

Sandwich-type photovoltaic cells of Al/dye/Au were fabricated as follows. At first, semitransparent aluminum films were prepared onto precleaned glass substrates by vacuum deposition at 1×10^{-4} Torr. Then the dye films were prepared on the aluminum-coated glass substrate with a transmittance at 500 nm of $10 \pm 3\%$ (Al thickness was 22 ± 3 nm) by spin-coating. Finally, a gold film with thickness of about 12 nm was formed on the dye films by vacuum deposition at 1×10^{-4} Torr. The slow evaporation rate of less than 0.02 nm s^{-1} was used to prevent the short-circuit of the cells. The photoactive area was defined to 0.25 cm^2. The thickness of the evaporated Al and Au films was monitored by an Ulvac CRTM-5000 oscillating quartz thickness controller, and the thickness and the mixing ratio of the spin-coating dye films were estimated from the amount and the density of dye on the substrate. The amount was determined by a Hitachi U-3210 UV−visible spectrometer after dissolving it in chloroform. The density of Zntpp determined pycnometrically with water−ethanol (3:7 by weight) was 1.3 g cm^{-3}. Because the appropriate solvent to measure the density of RhB which is soluble in any solvent was not found, we temporary use the value of Zntpp for RhB.

The action spectra were measured at a scan rate of 60 nm min^{-1}. The light intensity was normalized to 20 μW cm^{-2} transmitted through the Al or Au electrode. An optical neutral density filter was employed to illuminate the photocell with an approximately constant intensity at each wavelength, since the variation of the photocurrent with the illumination intensity is sublinear. For the measurement of the resistance of the solid films, the Au/dye/Au surface cell was employed. The interdigitated Au electrode, 150 μm wide and 207.7 mm long, was deposited on a quartz substrate before the dye film by spin-coating was formed on it with a thickness of about 50 nm. The resistivity was estimated from the slope of the dark current−voltage line obtained by applying a ramp bias of 2 V and simultaneously measuring the current. All electrical measurements were performed soon after preparation of the cell to avoid any change of the photovoltaic properties with age and were carried out in air at a temperature of 22 ± 3 °C and a humidity of $40 \pm 10\%$. The light source consisting of a 750 W halogen tungsten lamp and a Jasco CT-10 monochromator with a Jasco scanning controller SDM-25C was used. The light intensity was monitored by an Advantest TQ-8210 optical power meter with a silicon photocell. The photocurrent was measured by an Advantest R-8240 electrometer and was recorded by a Yokogawa Denki 3057 portable recorder. The bias was applied by a Hokuto Denko HB-104 function generator with a scan rate of 600 mV min^{-1} for the measurement of current−voltage curves.

Cyclic voltammetry was performed in an N_2-purged dichloromethane containing 0.1 mol dm^{-3} tetrabutylammonium perchlorate (TBAP), using a glassy carbon disk (diameter was 3 mm) as the working electrode, a Pt wire as the counter electrode, and Ag/0.1 mol dm^{-3} $AgNO_3$ in acetonitrile as the reference electrode. Potential control was carried out by using a Hokuto Denko HA-301 potentiostat and a Hokuto Denko HB-104 function generator. Cyclic voltammograms were recorded on a Yokogawa 3025 $X-Y$ recorder. The half-wave potential, or the redox potential, measured at a scan rate of 100 mV s^{-1}, was the average of the cathodic and anodic peak potentials and was described on the basis of the half-wave potential of ferrocenium ion/ferrocene(Fc^+/Fc). The absorption spectra of the dye film formed on a slide glass were recorded on a Hitachi U-3210 UV−visible spectrometer.

Results and Discussion

The solids of Zntpp and RhB behave as p-type and n-type organic semiconductors, respectively.[17,36] When the Al/Zntpp/Au cell is illuminated from the Al side, the short-circuit photocurrent action spectrum follows the absorption spectrum of Zntpp solid film as shown in Figure 2a. The smaller photocurrent due to the absorption by the Zntpp layer, which is a so-called optical filter effect, is observed at the Soret band when illuminated from the Au side. The photocurrent flows from the Au electrode to the Al electrode through the external circuit for irradiation from both sides. These indicate that the photocurrent originates from the charge separation of excited Zntpp at the potential gradient in the Zntpp near the Al/Zntpp interface. Such a potential is produced by contact of the p-type semiconducting Zntpp and the low work function of Al. On the other hand, when the Al/RhB/Au cell is illuminated from the Au side, the action spectrum follows the absorption spectrum of RhB as shown in Figure 2b. Owing to an optical filter effect of RhB, a smaller photocurrent is observed for the irradiation from the Al side than for the irradiation from the Au side. The photocurrent flowing from the Au to the Al through the external circuit is also obtained in the RhB solar cell. These indicate that the excited RhB is responsible for the photocurrent and that the potential gradient is produced by the contact of n-type semiconducting RhB and high work function of Au at the Au/

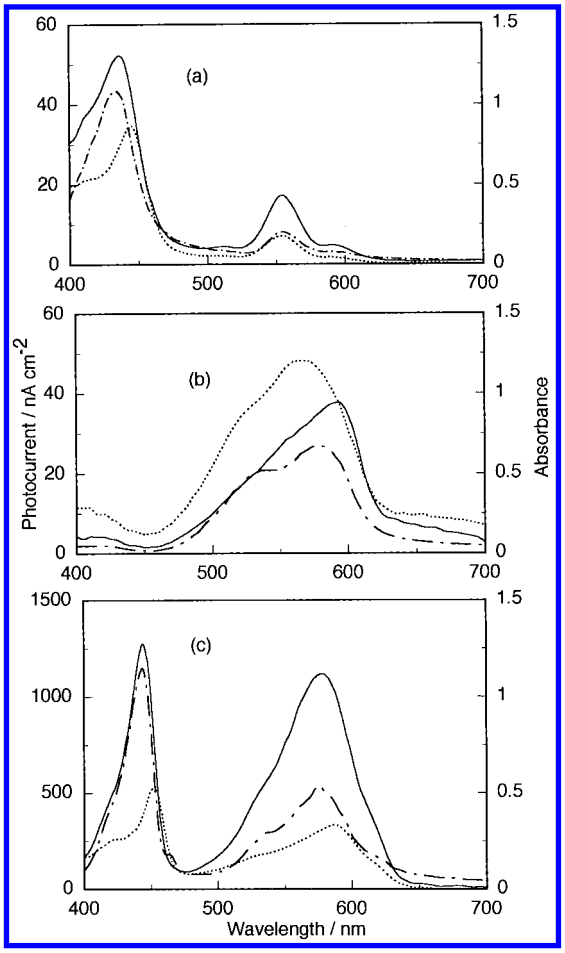

Figure 2. Photocurrent action spectra of Al/Zntpp (d = 36 nm)/Au (a), Al/RhB (d = 31 nm)/Au (b), and Al/mixed solid (R = 0.52)(d = 41 nm)/Au (c) cells, where d and R indicate the thickness of dye films and the molar ratio of porphyrin to total dye in the solid film, respectively. The incident light intensity at the Al/dye and Au/dye interfaces was normalized to 20 μW cm^{-2}. (−) represents irradiation from theAl side, (···) represents irradiation from Au side, and (− - −) represents absorption of dye film.

RhB interface. Therefore, which side of irradiation gives the larger photocurrent in the Al/dye/Au cell can be used for the judgment of whether the dye is a p-type or an n-type semiconductor. If the irradiation from Al side leads to a larger photocurrent, the dye is a p-type semiconductor. However, the larger photocurrent is observed by irradiation from the Au side for an n-type semiconducting dye. Figure 3 shows the current−voltage curves of Al/Zntpp/Au (a) and Al/RhB/Au (b) in the dark and under illumination. For all $J-V$ curves, clear rectification properties are not obtained because of the large resistance of the Zntpp and RhB solids. The unsaturated photocurrent with application of the negative bias to the Au electrode with respect to the Al electrode, namely, with application of the reverse-bias, is interpreted as a space−charge limitation in the large resistance of Zntpp and RhB. For the Al/Zntpp (thickness (d) is 31 nm)/Au cell, the short-circuit photocurrent quantum yield (ϕ) of 0.74%, open-circuit photovoltage (V_{oc}) of 0.80V, fill factor (ff) of 0.21, and energy conversion yield (η) of 0.04% are obtained when illuminated with the Soret peak wavelength of Zntpp (435nm) of 10.8 μW cm^{-2} intensity at the Al/Zntpp interface. For the Al/RhB(d = 42 nm)/Au cell, the values of ϕ = 0.17%, V_{oc} = 0.70 V, ff = 0.19, and η = 0.01% are obtained when illuminated with the absorption peak wavelength of RhB (570nm) of 28.4 μW cm^{-2} intensity at the Au/RhB interface. These values are calculated

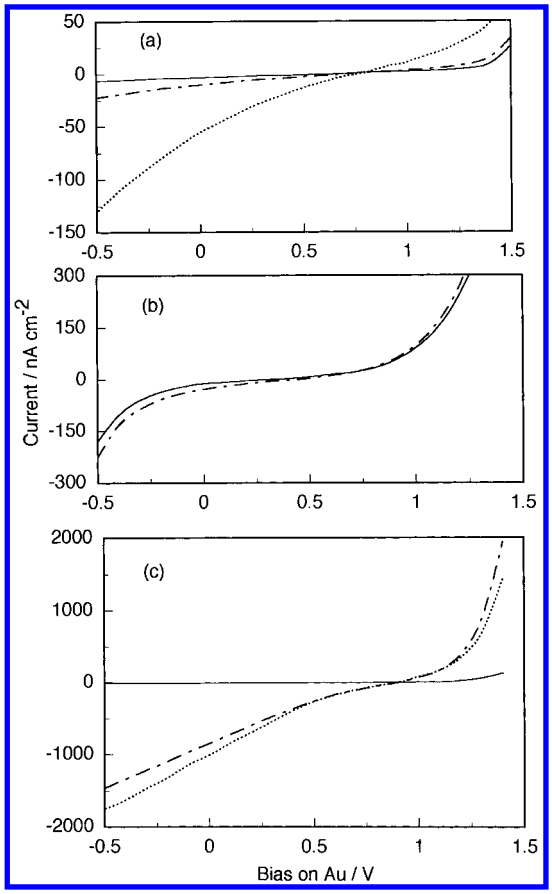

Figure 3. Dark current−voltage (−) and photocurrent−voltage characteristics for the irradiation by 440 nm (···) and 570 nm (− - −) monochromatic lights from the Al side in Al/Zntpp (d = 31 nm)/Au (a), from the Au side in Al/RhB (d = 42 nm)/Au (b), and from the Al side in Al/mixed solid (R = 0.57)(d = 33 nm)/Au (c) cells. The light intensity at Al/dye and Au/dye interfaces was normalized to 20 μW cm^{-2}.

by the following equations,

$$\phi = 1.24J_{sc}/(I_o\lambda) \quad (1)$$

$$\text{ff} = J_{max}V_{max}/(J_{sc}V_{oc}) \quad (2)$$

$$\eta = J_{sc}V_{oc}\text{ff}/I_o \quad (3)$$

where J_{sc} is the short-circuit photocurrent in units of nA cm^{-2}, I_o (μW cm^{-2}) is the light intensity at metal/dye interface, λ(nm) is the wavelength, and $J_{max}V_{max}$ is the maximum power output of the cell.

Figure 2c shows the photocurrent action spectra of the cell made up of the mixed solid of Zntpp and RhB and its absorption spectrum, where the mixing ratio (R) is 0.52 and is defined as the molar ratio of porphyrin to total dye. For the irradiation from the Al side, the action spectrum approximately follows the absorption spectrum and the photocurrent is enhanced compared with the cells made up of pure Zntpp and pure RhB. Furthermore, for the irradiation from the Au side, a large optical filter effect due to the mixed film is observed both at the Soret band of Zntpp and at the absorption band of RhB. This indicates that the mixed solid behaves as a p-type semiconductor. Figure 3c shows the current−voltage characteristics of an Al/mixed solid (R = 0.57) (d = 33 nm)/Au cell in the dark and under illumination. Compared with Figure 3a, the photo $J-V$ curve in Figure 3c shows a rapid increase of the forward-bias current where a rectification property under illumination is improved.

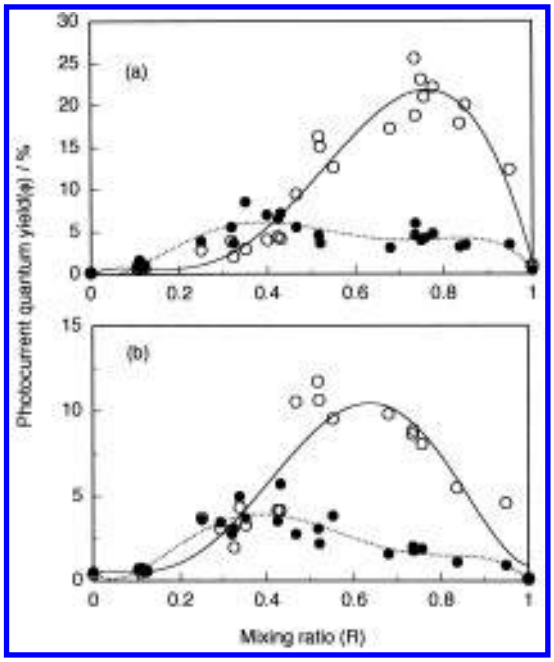

Figure 4. Relation between mixing ratio (R) and short-circuit photocurrent quantum yield (ϕ) at Soret band peak of Zntpp solid (a) (433−443 nm, $I_o = 13 \pm 3$ μW cm^{-2}) and absorption peak of RhB (b) (570 nm, $I_o = 35 \pm 4$ μW cm^{-2}) for Al/mixed solid of Zntpp and RhB ($d = 35 \pm 5$ nm)/Au cells, where I_o is the light intensity transmitted through the metal electrodes. ○ represents irradiation from Al side, and ● represents irradiation from Au side.

The result implies that the resistance of the mixed solid film is reduced by 2 orders of magnitude. This is one reason for the enhanced photocurrent in Zntpp−RhB cell. Since the dark series resistance of the cell estimated soon after illumination in the absorbance region of Zntpp or RhB was about half compared to that of the cell that has been standing for a long time in the dark, the photogenerated electrons may be quickly trapped in rather deep traps from which they are slowly released in the dark. The values of $\phi = 14.7\%$, $V_{oc} = 0.90$ V, ff = 0.18, and $\eta = 0.82\%$ are obtained when the sample is illuminated with 440 nm monochromatic light of 14.7 μW cm^{-2} intensity at the Al/dye interface, and the values of $\phi = 9.1\%$, $V_{oc} = 0.90$ V, ff = 0.19, and $\eta = 0.72\%$ are obtained when the sample is illuminated with 570 nm monochromatic light of 32.4 μW cm^{-2} intensity.

Figure 4 shows the dependence of the photocurrent quantum yield (ϕ) at the Soret peak of Zntpp (433−443 nm) (a) and at the absorption peak of RhB (570 nm) (b) on the mixing ratio (R) (molar ratio of porphyrin to total dye, $R = 0$ for pure RhB and $R = 1$ for pure Zntpp). The ϕ value for the irradiation from the Al side is larger than that from the Au side above the R value of 0.3−0.4, and a maximum is obtained at $R = 0.5$−0.8; that is, as Zntpp is mixed into the RhB solid in the Al/RhB/Au cell, the conductance changes from an n-type to a p-type and the photocurrent originating from both the excited RhB and Zntpp is remarkably enhanced. On the other hand, the V_{oc} value is 0.8−1.1 V, that is, it is nearly constant over all R range.

The Soret peak of Zntpp at 433 nm is largely shifted to longer wavelength by adding a small amount of RhB to the Zntpp solid, and its peak around 443 nm is observed at $R = 0.5$−0.7. The R dependence of the Soret peak wavelength of Zntpp in the mixed film is shown in Figure 5a. Such a large shift indicates that a ground-state complex with large electronic interaction is formed between Zntpp and RhB molecules. Figure 5b shows the R dependence of the extinction coefficient (α) for the mixed

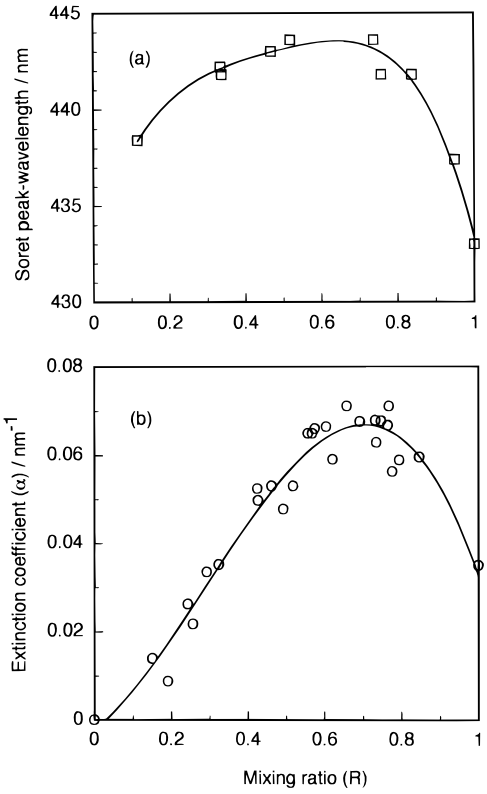

Figure 5. Relation between mixing ratio (R) and Soret peak wavelength of Zntpp in mixed solid of Zntpp and RhB (a) and R dependence of the extinction coefficient (α) at 443 nm (b).

film at 443 nm. The α is defined by the following equation,

$$I = I_o \exp(-\alpha d) \tag{4}$$

where I and I_o denote the transmitted and incident light intensities, respectively, and d is the film thickness. (The spin-coating dye film produced on the precoated semitransparent Al was employed for the exact estimation of α.) Since the α value at 443 nm has a maximum near $R = 0.7$, the ground-state complex exists most near this R value. The complex is maybe formed by the coordination of the oxygen or nitrogen atom in RhB to the zinc ion in Zntpp because the mixed solid of RhB and the metal-free porphyrin (H_2tpp: 5,10,15,20-tetraphenylporphyrin) hardly exhibit the shift of the Soret peak of H_2tpp.

Figure 6 shows cyclic voltammograms of Zntpp, RhB, and the mixture in dichloromethane. The redox wave of Zntpp in the mixed solution is reversible as shown in Figure 6c when the potential of the working electrode is scanned in the range −0.25−0.3 V vs Fc^+/Fc, but it becomes irreversible by scanning to more than 0.3 V because of a successive reaction. The first oxidation potential of Zntpp in the mixed solution (0.09V vs Fc^+/Fc) is largely shifted to the negative potential compared with that in the pure Zntpp solution shown in Figure 6a (0.28 V). Furthermore, the wave assigned to the RhB^+/RhB redox reaction in the mixed solution shown in Figure 6c is more reversible than that in the pure RhB solution shown in Figure 6b, but the oxidation potential (0.85 V) does not change by mixing Zntpp. These indicate that a ground-state complex is formed between Zntpp and RhB molecules in a noncoordination solvent such as dichloromethane and that an electronic interaction between their molecules gives a large influence for the oxidation properties. On the other hand, the reduction potential of the pure RhB and the pure Zntpp as well as the shape of their redox waves are not influenced by mixing Zntpp with RhB. (The first reduction potentials of RhB and Zntpp are −1.63 and −1.84 V, respectively.)

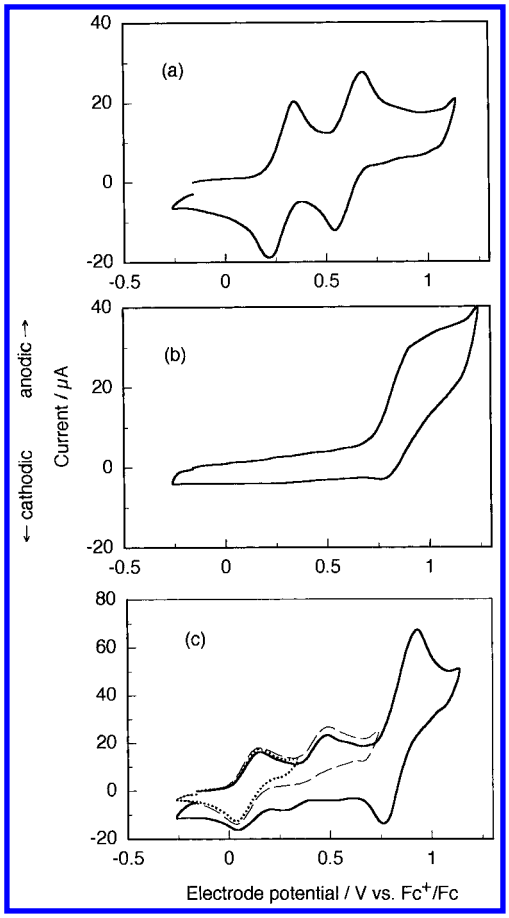

Figure 6. Cyclic voltammograms of 1×10^{-3} mol dm^{-3} Zntpp (a), 1×10^{-3} mol dm^{-3} RhB (b), and mixture of 1×10^{-3} mol dm^{-3} Zntpp and 2×10^{-3} mol dm^{-3} RhB (c) in dichloromethane containing 0.1 mol dm^{-3} TBAP.

The similarity between Figures 4a and 5b suggests that an excited state of the complex has a major role for the photocurrent generation of the mixed solid. The Zntpp and RhB constituting its complex can act as a donor and an acceptor, respectively, as inferred from their redox potentials. Therefore, the photoinduced charge-transfer state (CT state) may be formed by a partial charge transfer from Zntpp to RhB when the Zntpp−RhB complex is photoirradiated at either wavelength of the Soret peak of Zntpp (433−443 nm) or the absorption peak of RhB (570 nm). The charge separation effectively occurs from its CT state in the intrinsic electric field produced at the photoactive metal/dye interface, and a larger photocurrent is consequently obtained.

The R dependence of the specific conductivity of the mixed solid after standing for a long time in the dark is shown in Figure 7. (The resistance of Au/RhB/Au and Al/RhB/Al surface-type cells was approximately same despite a blocking contact between the Au electrode and the n-type RhB solid because the resistance of the RhB solid was much larger than that arising from the blocking contact. Therefore, all resistance was measured by Au/dye/Au surface-type cells. The Au electrode is preferably used because of its stability in air rather than Al electrode.) The specific conductivities of pure RhB and Zntpp solids are about 2×10^{-9} and 3×10^{-11} S cm^{-1}, respectively. Larger conductivity of $(3-7) \times 10^{-9}$ S cm^{-1} is obtained in the range $R = 0.6-0.8$, where the Zntpp−RhB ground-state complex is formed most. Since the complex is very easily oxidized as mentioned in the previous section, holes as the majority carrier tend to be produced in the mixed solid because of the easy electron transfer from the complex to the absorbed oxygen gas. This is one of the reasons that the mixed dye cell

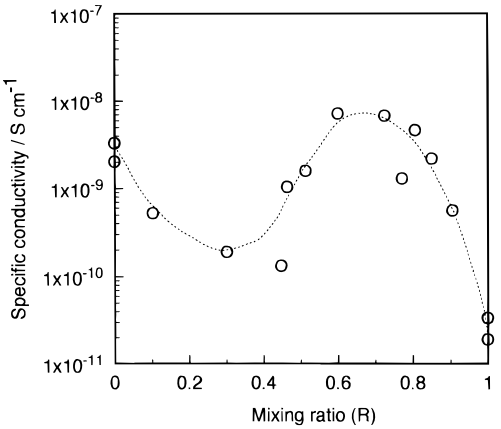

Figure 7. Relation between mixing ratio (R) and specific conductivity for mixed solid of Zntpp and RhB.

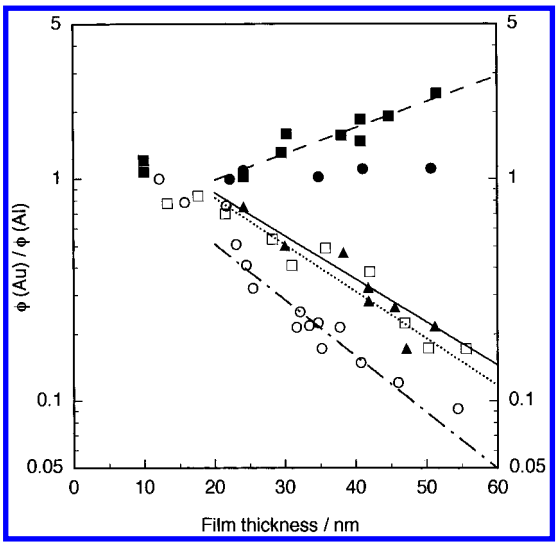

Figure 8. Plot of the value of ϕ(Au)/ϕ(Al) at the Soret peak wavelength of Zntpp as a function of the thickness of dye film. Symbols are the experimental values, and lines are estimated by calculation: (■) $R = 0.25 \pm 0.03$; (- - -) $W_{ap} = 8$ nm, $L_{exc} = 14$ nm; (●) $R = 0.4 \pm 0.03$; (▲) $R = 0.55 \pm 0.03$; (•••) $W_{ap} = 7$ nm, $L_{exc} = 10$ nm; (○) $R = 0.75 \pm 0.03$; (− - −) $W_{ap} = 3$ nm, $L_{exc} = 6$ nm; (□) $R = 1$; (−) $W_{ap} = 10$ nm, $L_{exc} = 6$ nm.

shows a much higher photocurrent. On the other hand, the conductivity exhibits a minimum at $R = 0.3-0.4$, where the photoactive interface changes from the Au/dye to the Al/dye. This suggests that the holes as the majority carrier of the solid consisting of the ground-state complex and the electrons as that of the RhB are electrically neutralized by mixing their solids. The mixed solids consequently exhibit a p-type conductance above R of about 0.4 and an n-type conductance below the R value.

It is expected that the optical filter effect observed by irradiating from the side of the ohmic interface becomes large as the depletion layer becomes narrow and the thickness of dye film becomes thick because the dye layer prevents the approach of photons to the photoactive interface, and/or as it becomes difficult for excitons to diffuse to the photoactive interface because of the short diffusion length of excitons. The dye solid with high carrier density should have a narrow depletion layer because of effective charge compensation for the blocking contact between metal and dye. Figure 8 shows the dependence of the optical filter effect at the various mixing ratios on the film thickness. The effect is represented by ϕ(Au)/ϕ(Al). ϕ-(Au) is the short-circuit photocurrent quantum yield at the Soret peak of Zntpp for the irradiation from the Au side, and ϕ(Al) is

TABLE 1: Apparent Barrier Width (W_{ap}) and Exciton Diffusion Length (L_{exc}) for the Metal/Mixed Solid of Zntpp and RhB Schottky Barrier Cell

mixing ratio	metal	λ^a (nm)	α^b (nm)	W_{ap} (nm)	L_{exc} (nm)
1	Al	433	0.0546	10 ± 2	6 ± 4
0.75	Al	443	0.0695	3 ± 2	5 ± 4
0.55	Al	443	0.0594	7 ± 6	10 ± 9
0.4		443	0.0466		
0.25	Au	440	0.025	7 ± 1	15 ± 1

[a] Wavelength of incident light. [b] Extinction coefficient defined by eq 4 in text.

that for the irradiation from the Al side. The ϕ(Au)/ϕ(Al) value is less than unity above $R = 0.5$ and more than unity below $R = 0.3$. This indicates that the photoactive interface changes from the Au/dye to the Al/dye at $R = 0.3-0.5$. The largest effect is obtained near $R = 0.75$ because its mixed solid has a higher hole density, as shown in Figure 7, and the depletion layer is consequently narrow. On the other hand, the effect is hardly observed near $R = 0.4$ because its mixed solid has a lower hole density and the depletion layer is consequently wide.

Estimating the width of the depletion layer at the photoactive interface and the diffusion length of excitons is important for clarifying the mechanism of the photocarrier generation at the Schottky barrier. The apparent width of the Schottky barrier (W_{ap}) and the exciton diffusion length (L_{exc}) are estimated by the following equation proposed by Yamashita et al.[37] that makes use of the optical filter effect due to the dye film,

$$\phi(\mathrm{Au})/\phi(\mathrm{Al}) = \int_0^d\int_0^d \Phi_a(x)\Phi_b(x') \exp[-\alpha(d-x) - (x-x')^2/{L_{exc}}^2]\, dx\, dx' / \int_0^d\int_0^d \Phi_a(x)\Phi_b(x') \exp[-\alpha x - (x-x')^2/{L_{exc}}^2]\, dx\, dx' \quad (5)$$

where the meaning of the many symbols is described below. $\Phi_a(x)$ is the quantum efficiency for the generation of excitons at a distance x from the photoactive interface, and the excitons are assumed to reach a point x' in proportion to $\exp[-(x - x')^2/L_{exc}^2]$ under stationary illumination. Furthermore, $\Phi_b(x')$ is the quantum efficiency of the carrier generation from the excitons. d and α denote the thickness of the dye film and the extinction coefficient, respectively, defined by the eq 4. It is assumed that $\Phi_a(x)$ is nearly equal to unity and $\Phi_b(x')$ is proportional to the electric field $E'(x')$ in the space−charge region,

$$E'(x') = E'_{max} \exp(-x'/W_{ap}) \quad (6)$$

where E'_{max} is the maximum field at the photoactive interface; that is, the observed effect is interpreted in terms of the following theoretical model. The photogenerated charge carriers are attributed to the dissociation of excitons diffusing toward the Schottky barrier, and the quantum efficiency of carrier generation is not constant over the dye layer but exponential at the barrier, and furthermore, the W_{ap} is the distance where the electric field becomes 1/e of the maximum field at the metal/dye interface. The W_{ap} and the L_{exc} in eqs 5 and 6 are given by numerical calculations using the Monte Carlo method with a computer. Figure 8 shows further the calculated lines of the optical filter effect at various mixing ratios. Since the estimated lines by the proposed model approximately agree with the experimental plots as shown in Figure 8, its model seems reasonable. However, the experimental plots at $R = 0.4$ do not fit the theoretical line because of the very small optical filter effect. Table 1 summarizes the estimated values of W_{ap} and L_{exc} for the various R values. The L_{exc} value somewhat increases with increasing RhB ratio, and the minimum W_{ap} value of 3 ± 2 nm is obtained at $R = 0.75$ with the largest optical filter effect. The fact that the W_{ap} exhibits the minimum at $R = 0.75$ seems reasonable because the conductivity, or the hole density, is largest near this mixing ratio as shown in Figure 7.

Because the open-circuit photovoltage (V_{oc}) approximately indicates the difference between the Fermi levels of the metal constituting the photoactive interface and the flat-band state of the dye, the potential corresponding to the V_{oc} value exists at the Schottky barrier under the short-circuit condition. Therefore, we can estimate the magnitude of the intrinsic electric field in the depletion layer by V_{oc} and W_{ap}. Since V_{oc} is a nearly constant value of 0.8−1.1 V regardless of the R value and the minimum W_{ap} of 3 ± 2 nm is obtained at $R = 0.75$, the potential slope at the Al/dye interface is steepest at the R value of about 0.75. Therefore, the excitons in the Schottky barrier most efficiently dissociate to free carriers at this mixing ratio. The largest photocurrent quantum yield is consequently obtained with the mixed solid of $R = 0.75$, although its solid has the short exciton diffusion length of 5 ± 4 nm. On the other hand, the potential slope at the photoactive metal/dye interface does not simply change by decreasing the R value below $R = 0.75$. The potential slope indicates a minimum at $R = 0.4$ because the conductivity, or the carrier density, indicates the minimum value at $R = 0.3-0.4$ as shown in Figure 7, and consequently, the depletion layer has a maximum width at $R = 0.4$ as shown by the smallest optical filter effect in Figure 8. Nevertheless, the ϕ value merely decreases with decreasing mixing ratio below $R = 0.7$ as shown in Figure 4a. Thus, the photocurrent is not only governed by the potential slope at the Schottky barrier. The R dependence of the ϕ value is similar to that of the concentration of the ground-state complex; that is, the photoinduced CT state of the complex easily dissociates to free carriers even by a small intrinsic electric field in the depletion layer, in contrast with the excitons of the pure RhB and Zntpp molecules.

In conclusion, a large amount of ground-state complex with a large electronic interaction is produced by mixing Zntpp and RhB molecules, and the specific conductivity of the mixed solid becomes large compared with the pure Zntpp and RhB solids. Therefore, the potential slope in the Schottky barrier becomes steep in the mixed solid, and also a large amount of photoinduced CT state is easily produced. These factors are the reason that a larger photocurrent quantum yield is observed with the organic solar cell made up of the mixed solid than those made up of the pure Zntpp and RhB solids.

Acknowledgment. The present research was partly supported by YAZAKI Memorial Foundation for Science and Technology.

References and Notes

(1) Tang, C. W. *Appl. Phys. Lett.* **1986**, *48*, 183.
(2) Bolton, J. R. *Science* **1978**, *202*, 705.
(3) Tang, C. W.; Albrecht, A. C. *Nature* **1975**, *254*, 507.
(4) Corker, G. A.; Lundstrom, I. *J. Appl. Phys.* **1978**, *49*, 686.
(5) Dodelet, J. P.; Le Brech, J.; Chapados, C.; Leblanc, R. M. *Photochem. Photobiol.* **1980**, *31*, 143.
(6) Jones, R.; Tredgold, R. H.; O'Mullane, J. E. *Photochem. Photobiol.* **1980**, *32*, 223.
(7) Lawrence, M. F.; Dodelet, J. P.; Dao, L. H. *J. Phys. Chem.* **1984**, *88*, 950.
(8) Desormeaux, A.; Max, J. J.; Leblanc, R. M. *J. Phys. Chem.* **1993**, *97*, 6670.
(9) Lawrence, M. F.; Dodelet, J. P.; Ringuet, M. *Photochem. Photobiol.* **1981**, *34*, 393.
(10) Diarra, A.; Hotchandani, S.; Max, J. J.; Leblanc, R. M. *J. Chem. Soc., Faraday Trans. 2* **1986**, *82*, 2217.
(11) Fujihira, M.; Sakomura, M.; Kamei, T. *Thin Solid Films* **1989**, *180*, 43.

(12) Akiyama, K.; Nishikawa, S.; Ueyama, S.; Isoda, S. *Jpn. J. Appl. Phys*. **1995**, *34*, 3942.
(13) Loutfy, R. O.; Sharp, J. H. *J. Chem. Phys*. **1979**, *71*, 1211.
(14) Fan, F.; Faulkner, L. R. *J. Chem. Phys*. **1978**, *69*, 3334.
(15) Popovic, Z. D. *Appl. Phys. Lett*. **1979**, *34*, 694.
(16) Loutfy, R. O.; Sharp, J. H.; Hsiao, C. K.; Ho, R. *J. Appl. Phys*. **1981**, *52*, 5218.
(17) Kampas, F. J.; Yamashita, K.; Fajer, J. *Nature* **1980**, *40*, 284.
(18) Yamashita, K.; Kihara, N.; Shimidzu, H.; Suzuki, H. *Photochem. Photobiol*. **1982**, *35*, 1.
(19) Ghosh, A. K.; Feng, T. *J. Appl. Phys*. **1978**, *49*, 5982.
(20) Morel, D. L.; Stogry, E. L.; Ghosh, A. K.; Feng, T.; Purwin, P. E.; Shaw, R. F.; Fishman, C. *J. Phys. Chem*. **1984**, *88*, 923.
(21) Skotheim, T.; Yang, J. M.; Otvos, J.; Klein, M. P. *J. Chem. Phys*. **1982**, *77*, 6144.
(22) Popovic, Z. D.; Menzel, E. R. *J. Chem. Phys*. **1979,** *71*, 5090.
(23) Saito, T.; Sisk, W.; Kobayashi, T.; Suzuki, S.; Iwayanagi, T. *J. Phys. Chem*. **1993**, *97*, 8026.
(24) Kearns, D. R.; Tollin, G.; Calvin, M. *J. Chem. Phys*. **1960**, *32*, 1020.
(25) Loutfy, R. O.; Menzel, E. R. *J. Am. Chem. Soc*. **1980**, *102*, 4967.
(26) Chamberlain, G. A. *J. Appl. Phys*. **1982**, *53*, 6262.
(27) Harima, Y.; Yamamoto, K.; Takeda, K.; Yamashita, K. *Bull. Chem. Soc. Jpn*. **1989**, *62*, 1458.
(28) Takahashi, K.; Horino, K.; Komura, T.; Murata, K. *Bull. Chem. Soc. Jpn*. **1993**, *66*, 733.
(29) Hiramoto, M.; Sakaue, Y.; Yokoyama, M. *Bull. Chem. Soc. Jpn*. **1994**, *67*, 2011.
(30) Takahashi, K.; Nanbu, H.; Komura, T.; Murata, K. *Chem. Lett*. **1993**, 613.
(31) Takahashi, K.; Hashimoto, K.; Komura, T.; Murata, K. *Chem. Lett*. **1994**, 269.
(32) Takahashi, K.; Nakatani, S.; Yamaguchi, T.; Komura, T.; Ito, S.; Murata, K. *Sol. Energy Mater. Sol. Cells*, in press.
(33) Deisenhofer, J.; Epp, O.; Miki, K.; Huber, R.; Michel, H. *J. Mol. Biol*. **1984**, *180*, 385.
(34) Adler, A. D.; Longo, F. R.; Finarelli, J. D.; Assour, J.; Korsakoff, L. *J. Org. Chem*. **1967**, *32*, 476.
(35) Adler, A. D.; Longo, F. R.; Kampas, F.; Kim, L. *J. Inorg. Nucl. Chem*. **1970**, *32*, 2443.
(36) Kudo, K.; Moriizumi, T. *Jpn. J. Appl. Phys*. **1981**, *20*, L553.
(37) Yamashita, K.; Harima, Y.; Iwashima, H. *J. Phys. Chem*. **1987**, *91*, 3055.